Unusual Patch-matrix Organization in the Retrosplenial Cortex of the *Reeler* Mouse and *Shaking Rat Kawasaki*

Noritaka Ichinohe[1,6], Adrian Knight[1], Masaharu Ogawa[2], Toshio Ohshima[3], Katsuhiko Mikoshiba[3, 7], Yoshihiro Yoshihara[4, 8], Toshio Terashima[5], Kathleen S. Rockland[1, 9]

[1]Laboratory for Cortical Organization and Systematics, [2]Laboratory for Cell Culture Development, [3]Laboratory for Developmental Neurobiology, and [4]Laboratory for Neurobiology of Synapse, RIKEN, Brain Science Institute, Wako, Saitama 351-0198, Japan, [5]Department of Anatomy and Developmental Neurobiology, Kobe University Graduate School of Medicine, Chuo-ku, 7-5-1 Kusunoki-cho, Kobe 650-0017, Japan, [6]Graduate School of Medicine, Kyoto University, Kyoto 606-8501, Japan, [7]Department of Molecular Neurobiology, Institute of Medical Science, University of Tokyo, Minato-ku, Tokyo, Japan, [8]Core Research for Evolutional Science and Technology, Japan Science and Technology Agency, Osaka 560-0082, Japan and [9]Graduate School of Science and Engineering, Saitama University, Sakura-ku, Saitama-shi, Saitama, 338-8570, Japan

Correspondence author:

Noritaka Ichinohe, M.D., Ph.D.

Laboratory for Cortical Organization and Systematics

RIKEN, Brain Science Institute

2-1 Hirosawa, Wako-shi, Saitama 351-0198 Japan

TEL: +81-48-462-1111 (ext. 7119)

FAX: +81-48-467-6420

E-mail: nichinohe@brain.riken. Jp

Running Title: Patch-matrix in the reelin-deficient mutant cortex

The rat granular retrosplenial cortex (GRS) is a simplified cortex, with distinct stratification and, in the uppermost layers, distinct modularity. Thalamic and cortical inputs are segregated by layers and in layer 1 co-localize, respectively, with apical dendritic bundles originating from neurons in layers 2 or 5. To further investigate this organization, we turned to reelin-deficient *reeler* mouse and *Shaking Rat Kawasaki*. We found that the disrupted lamination, evident in Nissl stains in these rodents, is in fact a patch-matrix mosaic of segregated afferents and dendrites. Patches consist of thalamocortical connections, visualized by VGluT2 or AChE. The surrounding matrix consists of corticocortical terminations, visualized by VGluT1 or zinc. Dendrites concentrate in the matrix or patches, depending on whether they are OCAM-positive (matrix) or –negative (patches). In wild-type rodents and presumably mutants, OCAM^{+} structures originate from layer 5 neurons. By double labeling for dendrites (filled by Lucifer Yellow in fixed slice) and OCAM immunofluorescence, we ascertained two populations in *reeler*: dendritic branches either preferred (putative layer 5 neurons) or avoided (putative supragranular neurons) the OCAM^{+} matrix. We conclude that input-target relationships are largely preserved in the mutant GRS, and that dendrite-dendrite interactions involving OCAM influence the formation of the mosaic configuration.

Keywords: cortical layer, cortical module, thalamocortical, corticocortical, dendritic organization, OCAM

Introduction

The rat granular retrosplenial cortex (GRS) ia a simplified, limbic cortex with a sparse layer 4. Pyramidal cell dendrites and their afferent inputs have a highly organized laminar and modular geometry. This is particularly prominent in layer 1, where apical dendritic bundles, from neurons in layer 2, interdigitate with the apical dendritic tufts from pyramidal neurons in layer 5 (Wyss et al., 1990; Kaneko et al., 2002; Ichinohe and Rockland, 2002; Ichinohe et al., 2003; Miro-Bernie et al., 2006). Thalamic afferents, visualized by tracer injections or anti-vesicular glutamate transporter 2 (VGluT2) immunohistochemistry, target the dendritic bundles from layer 2 neurons in layer 1a,b. Intracortical projections (visualized by VGluT1) target layer 5 apical dendritic tufts in layer 1b,c (Wyss et al., 1990; Kaneko et al., 2002, Miro-Bernie et al., 2006). Modularity is not evident in the subjacent layers, but the laminar complementarity of inputs persists. Layers 3 and 4 are positive for VGluT2, and layers 5 and 6 for VGluT1 (Kaneko et al., 2002).

In a study of the postnatal developmental time course of dendritic aggregation, we established a significant role in this organization for the cell adhesion molecule OCAM (Ichinohe et al., 2003). OCAM, localized mainly on dendrites of layer 5 neurons, exhibits a patchy distribution in layer 1 from as early as P3 in the rat. This predates the conspicuous dendritic aggregates of layer 2 neurons by 2 days. On this bases, therefore, OCAM has been proposed to have homophilic adhesive effects among dendrites of layer 5 neurons and repellent effects on the interposed dendrites of layer 2 neurons (Ichinohe et al., 2003). In addition, we found that OCAM can serve as a convenient reference marker for corticocortical afferents (co-localizing with OCAM[+] patches or layers) and thalamocortical afferents (corresponding to OCAM[-] patches or layers).

To further investigate this distinctive compartmental organization, we turned to the reelin-deficient mutant rodents, *reeler* mouse and *Shaking Rat Kawasaki (SRK)*. In these animals, the normal lamination is conspicuously disrupted, and dendrites are malpositioned

(Caviness and Rakic, 1978; Pinto Load and Caviness, 1979; Landrieu and Goffinet, 1981; Caviness et al., 1988; Aikawa et al., 1988; Terashima et al., 1992; Lambert de Rouvroit and Goffinet, 1998; Tabata and Nakajima, 2002; Kikkawa et al., 2003). We specifically wanted to address (1) how is the highly organized laminar and modular architecture of the GRS in the wild-type rodent transformed and 2) is there still evidence of dendrite-dendrite interactions, despite the dispersal of layer 5 pyramidal cells?

Table 1. Table showing distribution of molecules and neuronal components in OCAM[+] layers or compartments in wild-type and mutant rodents (See text for more detailed description of sublayers 1a, b, c and layer 2)

	wild-type		mutant	
	OCAM[+] strata (layer 1a, 5 and 6)	OCAM[-] strata (layer layer 1b,c, 2-4)	OCAM[+] matrix	OCAM[-] patch
VGluT1	+	-	+	-
VGluT2	-	+	-	+
Zn	+	-	+	-
AchE	-	+	-	+
YFP-H^{+} axons (presumably subiculum origin)	+	-	+	-
OCAM mRNA[+] cell body	+	-	+	-
OCAM[+] dendrites and somata (EM)	+	-	+	-
Dendritic branching	+ form layer 5 pyramids	-	+ presumptive layer 5 pyramidals	-
	- from layer 2 pyramids	+	- presumptive layer 2 pyramids	+

As expected, given the laminar dispersal in these mutants, there was no evidence of any micro-modularity, which might have been displaced from layer 1. Instead, both in *SRK* and *reeler*, immunohistochemistry for OCAM revealed a patch and matrix-like mosaic,

where large OCAM⁻ patches in the middle of the cortical thickness were embedded in an OCAM$^+$ matrix. The thalamic and cortical afferents maintained the same relationships to this patch-matrix configuration as in the wild-type rodents (Table 1). Further, by filling neurons with Lucifer-yellow in fixed slices of the *reeler* GRS, we ascertained that these can be grouped into two populations, with dendrites showing preference to either OCAM⁻ patches or the OCAM$^+$ matrix. From *in situ* hybridization and EM results, we conclude that the OCAM$^+$ group corresponded to layer 5 neurons. Thus, even in the disrupted laminar cortex of *reeler* and *SRK*, OCAM may exert neuronal population-dependent homophilic or repellent dendritic effects.

Materials and Methods

Experimental subjects

The following normal and mutant animals were used for this study: 1) Wild-type Wistar rats (> 3 months, purchased from Japan SLC, Hamamatsu, Japan), 2) Homozygotes for the *SRK* mutation (*SRK*/*SRK*; 5-6 months, generated by pairing Wistar strain heterozygotes at Kobe University School of Medicine), 3) B6C3Fe wild-type mice (> 3 months, maintained at BSI, RIKEN, originated from heterozygous B6C3Fe-*a/a-rl* adults, The Jackson Laboratory, Bar Harbor, Maine), 4) CB57/6J wild-type mice (purchased from Japan SLC, Hamamatsu, Japan), 5) Homozygous *reeler* mice (> 3 months, maintained at BSI, RIKEN, originated from heterozygous B6C3Fe-*a/a-rl* adults), 6) YFP-H mice (3-4 weeks, Feng et al., 2000; purchased from Jackson Laboratory, Bar Harbor, ME, and maintained at BSI, RIKEN), 7) *reeler*;YFP-H mutant mice (3 weeks; generated by mating YFP-H mouse with *reeler* mice and genotyped as previously described by Feng et al., 2000 and D'Arcangelo et al., 1997). All experimental protocols were approved by the Experimental Animal Committee of the

RIKEN Institute, and were carried out in accordance with the guidelines published in Guide for the care and use of laboratory animals (DHEW Publication. No. NIH 85-23, 1996).

Perfusion fixation

Nembutal (50 mg/kg) was used for anaesthetising the following animals: wild-type Wistar rats (n = 5), B6C3Fe (n = 2) and CB57/6J (n = 5) wild-type mice, *SRK* (n = 4), *reeler* mice (n = 8), YFP-H mice (n = 3), *reeler*;YFP-H mutant mice (n = 4). Animals were transcardially perfused, in sequence, with 0.9% saline and 0.5% sodium nitrite for 1 min, and 4% paraformaldehyde in 0.1 M phosphate buffer (PB, pH 7.3) for 10 min. Postfixation was performed using the same fixative for 2 hrs. For Zn histochemistry, we injected sodium sulfide (200 mg/kg) via the vena cava inferior 3 min before saline perfusate. Following fixation, Then, the brains were placed in 30% sucrose, and after sinking, were cut into 40-μm-thick sagittal or coronal sections on a freezing microtome.

Single and double immunofluorescence for OCAM, VGluT1 and VGluT2

Sections were pre-incubated for 1h with 0.1 M phosphate buffered saline (PBS, pH 7.3) containing 0.5% Triton X-100 and either 5% normal goat serum (PBS-TG) or normal donkey serum (PBS-TD) at room temperature. Serum species were chosen so as to match with the host animal of the secondary antibody. Then, the sections were incubated for 40-48 hrs at 4°C in either a mixture of two different antibodies or one antibody. The antibodies, raised from different animals in the case of double labeling, were chosen from the following: anti-VGluT1 polyclonal rabbit antibody (SYSY, Gottingen, Germany, 1:1,000), anti-VGluT2 polyclonal rabbit antibody (SYSY, Gottingen, Germany, 1:1,000), anti-VGluT2 polyclonal guinea pig antibody (Chemicon, Temecula, CA; 1:2,000), anti-OCAM polyclonal rabbit antibody (Yoshihara et al., 1997; 1:1,000), and anti-OCAM polyclonal goat antibody (R&D Systems, Minneapolis, MN; 1:300). Antibody combinations were (1) for OCAM (raised in goat) and either VGluT1 or VGluT2 (raised in rabbit), (2) for OCAM (raised in rabbit) and

VGluT2 (raised in guinea pig). Finally, the sections were incubated for 1.5 hrs in either PBS-TG or PBS-TD containing the suitable combination of secondary antibodies. These were chosen from the following: Alexa Fluor 488-conjugated anti-rabbit IgG donkey polyclonal antibody (Molecular Probes, Eugene, OR; 1:200); Alexa Fluor 594-conjugated anti-goat IgG donkey polyclonal antibody (Molecular Probes, Eugene, OR; 1:200); Alexa Fluor 596-conjugated anti-rabbit IgG goat polyclonal antibody (Molecular Probes, Eugene, OR; 1:200); Alexa Fluor 488-conjugated anti-guinea pig IgG goat polyclonal antibody (Molecular Probes, Eugene, OR; 1:200).

Double labeling combining AChE histochemistry and immunofluorescence for VGluT2

AChE histochemistry was performed following Tsuji's method (1998) with slight modification. After washing in a mixture containing 1 ml of 0.1 M citrate buffer (pH 6.2) and 9 ml 0.9% saline (CS), sections were incubated with CS containing 3 mM $CuSO_4$, 0.5 mM $K_3Fe(CN)_6$ and 1.8 mM acetylthiocholine iodide for 1 h. After rinsing in PB, sections were intensified in PB containing 0.05% DAB and 0.03% nickel ammonium sulfate. After washing in PB, we further carried out immunofluorescence for VGluT2, described above.

Double labeling combining Zn histochemistry and immunofluorescence for VGluT2

For the detection of synaptic zinc, sulphide precipitation (as ZnS) followed by silver amplification was used (Miro-Bernie et al., 2006). Sections were immersed in a solution made of 33% Arabic gum, IntenSE M silver Enhancement kit (Amersham International, Bucks, UK) component A and component B, freshly mixed before use in a 2:1:1 ratio, and developed for 180 min in the dark. Then sections were thoroughly rinsed in PB and in 5% thiosulphate-0.05 M PB for 12 min and processed for immunofluorescence for VGluT2 (described above).

In situ hybridization for mouse OCAM

PCR primers for mouse OCAM (5'-TCACCAAGCAAGATGATGGA-3' and 5'-AAAATTGGTGCCAATCAAGC-3') were designed based on the nucleotide sequence of mouse OCAM (GenBank No. NM_010954). The cDNA fragments were obtained by reverse transcriptase-polymerase chain reaction (RT-PCR) from mouse cDNA. PCR fragments were ligated into the pBluescript II (KS $^+$) vector. The plasmid was linearized with Asp718 or XhoI and used as the template for antisense or sense cRNA probes. The digoxigenin (DIG)-dUTP labeling kit (Roche, Basel, Switzerland) was used for *in vitro* transcription.

Two wild-type and two *reeler* mice were used for *in situ* hybridization for OCAM. Animals were perfused as above. Sections were cut (in the coronal plane, at 30 µm thickness) by using a sliding microtome, and were washed in PB, and postfixed with 4% paraformaldehyde in PB for 10 min. After washing in PB, sections were treated with 1 µg/mL proteinase K for 10 min at 37 ℃, acetylated, and then incubated in hybridization buffer containing 0.5−1.0 µg/mL DIG-labeled riboprobes at 60 ℃. The sections were sequentially treated for 15 min at 55 ℃ in 2 X standard sodium citrate (SSC)/50% formamide/0.1% N-lauroylsarcosine, twice; for 30 min at 37 ℃ in RNase buffer (10 mM Tris−HCl, pH 8.0, 1 mM EDTA, 500 mM NaCl) containing 20 µg/mL RNase A (Sigma, St. Louis, MO, USA); for 15 min at 37 ℃ in 2 X SSC/0.1% N-lauroylsarcosine, twice; for 15 min at 37 ℃ in 0.2 X SSC/0.1% N-lauroylsarcosine, twice. The hybridized probe was detected by an anti-DIG antibody conjugated with horseradish peroxidase (Roche Diagnostics, 1:2000 in the blocking buffer) for 2-5 h at room temperature. After washing in TNT (0.1 M Tris-HCl, pH 7.5, 0.15 M NaCl, 0.1% Tween 20) 3 times for 15 min, the sections were treated with 1:50 diluted TSA-Plus (dinitrophenol [DNP]) reagents for 30 min according to the manufacturer ' s instruction (Perkin-Elmer, Wellesley, MA), and the DIG signals were converted to DNP signals. After washing in TNT 3 times for 10 min, the sections were incubated for 2-5 h at room temperature with an anti-DNP antibody conjugated with Alexa Fluor 488 (Molecular

Probes; 1:100) in 1% blocking buffer for the fluorescence detection). Control of hybridization with sense strand-labeled riboprobes showed no hybridization signal. The sections adjacent to those stained for *in situ* hybridization were also stained for immuno fluorescence for OCAM as described above.

Ibotenic acid injection into subiculum of YFP-H mouse

Three YFP-H mouse (4-5 weeks) were anaesthetised with Nembutal (50 mg/kg). In an aseptic surgical procedure, 10 injections of ibotenic acid (10 mg/ml, 0.05 μl each) were made unilaterally in the subiculum by stereotaxic localization (Hof et al., 2000). A 10 μl Hamilton syringe (Reno, NV) with a 32 gauge needle was lowered according to posterior (P), lateral (L), and vertical (V) coordinates in relation to bregma and the skull surface: P, range -3.3 mm – -4.4 mm; L, range 1.6 mm – 3.5 mm; and V, range 1.5 mm – 4.0 mm. Ibotenic acid solution was delivered over 1 min after a 1 min wait. Five days later, animals were re-anesthetized, perfused as described above, and brains were processed for VGluT2 immunofluorescence using Alexa Fluor 594-conjugated secondary antibody (described above).

OCAM immunoelectron microscopy

OCAM immunoelectron microscopy was carried out as previously described (Ichinohe et al., 2003). In short, vibratome coronal sections of 50 μm thickness were prepared from two of the following animals, wild-type mice and rats, *reeler* mice and *SRK.* Perfusion fixation was performed using 4% paraformaldehyde with 0.1% glutaraldehyde in PB with post-fixation for 2 hrs. Tissue including the GRS was trimmed out to facilitate the processing. Sections were incubated in 20% sucrose, and then were freeze-thawed with liquid nitrogen. Sections were incubated for 1 hr with PBS containing 5% normal goat serum (PBS-G) at room temperature, and then for 24 hrs at 4°C with PBS-G containing rabbit polyclonal anti-OCAM antibody (see

above, 1:10,000). After rinsing, signals were visualized with ABC-DAB method. Sections were osmicated, dehydrated and flat-embedded in resin (Araldite M; TAAB, Aldermaston, UK). From the plastic sections, we further trimmed out both $OCAM^+$ matrix and $OCAM^-$ patch, which was easily identified, from mutant rodents, and $OCAM^+$ layer 5 from wild-type rodents. Ultrathin sections were collected on formvar-coated, single-slot grids, and examined with an electron microscope (JEM 2000-EX; JEOL, Tokyo, Japan). For quantification, electron micrographs were taken at a magnification of 20,000 from randomly selected fields that included OCAM-labeled elements in the neuropil. Total 100 digital fields were recorded from ultrathin sections (4 μm interval in order to avoid to count the same structures) of one tissue sample from two animals of each rodent type examined. On each micrograph, OCAM-labeled profiles were identified based on standard ultrastructural criteria (Peters et al., 1991).

Lucifer Yellow filling of neurons in wild-type and* reeler *mice

Four wild-type mice and five *reeler* mice were used. Animals were deeply anaesthetized as described above. Brains were removed from the skull, and post-fixed for 30 minutes in 4% paraformaldehyde in PB. The 300 μm coronal sections of the GRS were cut by vibratome, and mounted onto black Millipore filter papers. The mounted sections were then immersed in a PB solution containing the nuclear dye 4,6-diamidino-phenylindole (DAPI; Sigma, St. Louis, MO), for 1 hr. Glass pipettes (1 mm OD, World Precision Instruments, Sarasota, FL) were pulled on a Brown-Flaming P-97 micropipette puller (Sutter Instrument, Novato, CA). An impedance of 80 MΩ to 150 MΩ was considered optimal for injection. Pipettes were backfilled with 8% Lucifer Yellow CH dilithium salt (Sigma, St. Louis, MO) in 0.05M Tris buffer (pH 7.3). Filled pipettes were lowered toward the tissue chamber, by using a micromanipulator (Narishige, Tokyo, Japan). Pipettes were viewed under ultraviolet excitation (355-425nm), so that both the pipettes and the DAPI labeled section were

visualized together. The pipette tip was coarsely maneuvered using a 4x objective lens (Nikon Optiphot2-UD, Nikon, Tokyo, Japan). Then, with the finer resolution of a 20x objective lens individual cells were selected and penetrated. Following successful penetration, iontophoresis of Lucifer Yellow (LY) was achieved by passing a 10 nA positive current for approximately 1 min. Following multiple intracellular injections, the section was immersed in 4% paraformaldehyde in PB for 20 min. The 300 μm-thick sections were then re-sectioned on a freezing microtome at 50 μm thickness. The thinner sections were pre-incubated for 1h with PBS-TD, and then were incubated 40-48 hrs at 4$°$C in PBS-TD containing anti-LY polyclonal rabbit antibody (raised by Dr. David Pow, 1:40,000), and either anti-VGluT2 polyclonal guinea pig antibody (Chemicon, Temecula, CA; 1:2000) or anti-OCAM polyclonal goat antibody (R&D systems, Minneapolis, MN; 1:300). Finally, the sections were incubated for 1.5 hrs in PBS-TD containing Alexa Fluor 488-conjugated anti-rabbit IgG donkey polyclonal antibody (Molecular Probes, Eugene, OR; 1:200) and either Alexa Fluor 594-conjugated anti-guinea pig IgG donkey polyclonal antibody (Molecular Probes, Eugene, OR; 1:200) or Alexa Fluor 594-conjugated anti-goat IgG donkey polyclonal antibody (Molecular Probes, Eugene, OR; 1:200).

Data Analysis

The center-to-center distance of compartments visualized by Nissl staining and immunohistochemistry were measured on digitized images of 20 sections from two animals aided by Image J software (http://rsb.info.nih.gov/ij/; National Institute of Health, USA).

To analyze dendritic organization of LY-filled neurons in relation to patch and matrix compartments, high resolution images (3900 x 3090 pixels) of LY-filled tissues were taken using a Zeiss Axioskop 2 microscope (Zeiss, Jena, Germany). First, an 'overview' of the pattern of OCAM labeling was taken at 100x magnification, and cells randomly selected from successfully injected cells were then analysed at higher magnification (200x). Depth through the tissue was documented by taking 5 stepwise images (6 μm each step).(Given

the well-known shrinkage in the z-dimension, the thickness of 50 μm for microtomed, wet tissue became 30 μm for dehydrated and coverslipped tissue.) These images including LY-filled neurons were then stacked and aligned using Adobe Photoshop (Adobe Systems, San Jose, CA). Using these images, dendrites and cell bodies of the injected neurons were traced with Neurolucida Confocal software (MicroBrightField, Williston, VT). The borders of OCAM$^+$ matrix and OCAM$^-$ patches were drawn by the same system. The acquired data were analyzed with NeuroExplorer (MicroBrightField, Williston, VT). We measured the following morphological parameters for each selected neuron: 1) the total length of dendrite in the matrix, 2) the total length of dendrite in the patch, 3) total dendritic length and 4) the total length of dendrite in the matrix divided by the total dendritic length (M/T ratio). We defined neurons with an M/T ratio below 0.5 as patch-preferring neuron, and those with an M/T number greater than 0.5 as matrix-preferring neuron (see Results).

Since the M/T ratio may be strongly influenced by the 3-dimensonal configuration of the surrounding patch and matrix, we have attempted to compensate for this by computer-rotation of the reconstructed dendrites while holding constant the position of the cell body, using Adobe Photoshop. Rotation at 90, 180, and 270 degree were carried out against a fixed patch-matrix configuration (Fig. S1), and the M/T ratio was re-calculated for these three conditions. If dendrites of a neuron have preference to matrix, the M/T ratio of 0 degree position (original position) for this neuron should be high compared to the three rotated positions (90, 180, 270 degree), and *vice versa*. Statistical comparison between original position versus the three rotated positions was performed separately for groups of patch and matrix preference neurons using the Kruskal-Wallis test ($P < 0.05$).

Light microscopic photographs were taken on digital cameras (Axioscop2 and Axiocam, Carl Zeiss Vision, München-Hallbergmoos, Germany). Size, brightness, and contrast of images were adjusted to coincide with the real image, by using Photoshop software (Adobe Systems, San Jose, CA).

Nomenclature

Areal, laminar and nuclear boundaries were defined by using thionin for cell bodies, VGluT2 immunohistochemistry or AchE histochemistry. The nomenclature and abbreviations for cortical areas follow Paxinos & Watson (2004) for rats and Hof et al. (2000) for mice. For zinc-positive structures, we use the abbreviation Zn+ (no superscript, so as not to confuse with Zn^{2+}).

RESULTS

Cytoarchitecture of wild-type and mutant rodents

The GRS of the wild-type rodent shows a clear laminar organization (Fig. *1A, C*). In the wild-type rat, the GRS has a thick infragranular stratum (layers 5 and 6), with distinct large pyramidal neurons in layer 5; a thin, cell-sparse layer 4; thin, but clearly distinguishable layers 2 and 3; and a relatively thick layer 1.   Small, densely packed pyramidal neurons aggregate in layer 2. The laminar organization of wild-type mouse GRS is basically similar, except that the cell sparse layer 4 is harder to distinguish and the overall cortical thickness (about 1.0mm) is about half that of rat GRS (about 2.0 mm).

In the GRS of both *reeler* and *SRK*, the laminar structure is conspicuously disrupted (Fig. *1B, D*). In the position of layer 1, defined by its subpial location, there is a more cell-dense stratum, presumably corresponding to layer 6. This is consistent with the quasi-inverted disruption of the cortical organization, as described in the literature (Aoki et al., 2002; Yamamoto et al., 2003). Large cell bodies, likely to correspond to layer 5 pyramids of the wild-type phenotype, are scattered throughout the cortical thickness.   Aggregations of mainly small cells are apparent in the mid-cortical thickness. These aggregations are elongated in the pial to white matter plane, with a center-to-center distance (measured parallel to the pia) of 50-150 μm in *SRK* and 40-100 μm in *reeler* mouse.
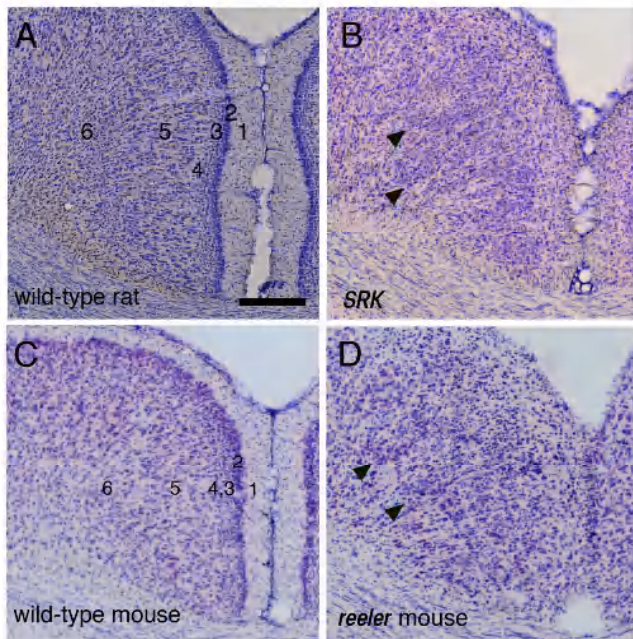
Figure 1. Cytoarchitecture of GRS in normal and mutant rodents, in Nissl-stained coronal sections. *A,* wild-type rat. *B, SRK. C,* wild-type mouse. *D, reeler* mouse. Aggregations of small cells can be seen in the middle stratum of mutant animals (arrowheads in *B, D*). Arabic numbers indicate layers. Note higher magnification in *C, D* (twice than in *A, B*). Scale bar, *A, B,* 300 μm; *C, D,* 150 μm.

Organization of OCAM and input specific markers in the GRS of wild-type and mutant rodents

In the wild-type rat and mouse, OCAM immunoreactivity is bistratified, with two dense bands, one in layer 1 (especially 1b, c) and another in layers 5,6 (Fig. 2*A, D*, Table 1). In wild-type rat, the superficial band (layer 1b,c) has a distinct notch-like appearance (Fig. 2*A*), but this is not evident in the mouse (Fig. 2*D*). (Dendritic bundling, as assayed by MAP2, is not obvious in the adult mouse, but can be discerned at P8 mice in which the *Escherichia coli lacZ* gene is integrated into the neurotrophin-3 locus, see Fig. 1*F* in Vigers et al., 2000). Double labeling for OCAM and VGluT2 (presumptive thalamocortical terminals; Fujiyama et al., 2001) showed that the expression patterns of OCAM and VGluT2 are generally complementary, except for layer 2, which is devoid of both molecules (Fig. 2*A-C*, Table 1). In contrast, double labeling for OCAM and VGluT1 (presumptive corticocortical terminals; Fujiyama et al., 2001) showed co-localization, again except for layer 2, which is devoid of both molecules (Fig. 3*A-D*, Table 1). From these results we conclude that, in wild-type

14

rodent GRS, VGluT2^{+} thalamocortical and VGluT1^{+} corticocortical terminals have preferential distributions and that these are strongly associated with OCAM distribution (see also: Wyss et al., 1990; Kaneko et al., 2002; Ichinohe et al., 2003; Miro-Bernie et al., 2006).
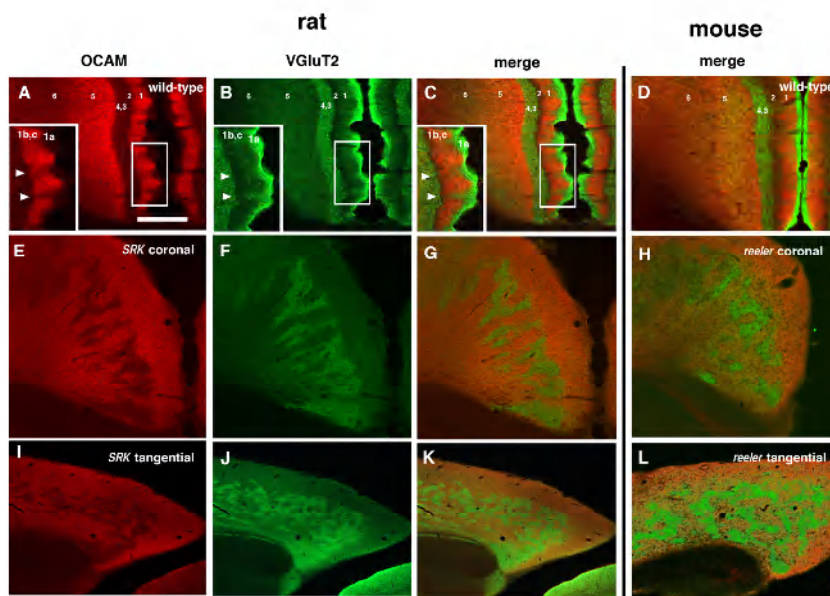

Figure 2. Architectonics of wild-type and mutant GRS, visualized by immunohistochemistry for OCAM and VGluT2 (presumptive thalamocortical terminations). *A-D,* Coronal sections reacted for OCAM and VGluT2 from wild-type rat (*A-C*) and wild-type mouse (*D*). For the sake of space, only the merged image is shown for mouse in this figure. OCAM-ir in the wild-type rat (*A*) is bistratified, with one superficial band in layer 1b, c and another, deeper band in layers 5, 6. Note notch-like appearance in layer 1 (inset in *A*). Similarly, VGluT2 concentrates in two bands, but these correspond to layer 1a and layers 3, 4 (*B*). Double immunofluorescence for OCAM and VGluT2 directly demonstrates this complementary relationship (*C*). Layer 2 has low levels of both OCAM and VGluT2. Insets in *A-C* are higher magnification from the white boxes. Arrowheads point to corresponding locations. In the wild-type mouse (*D*), no modular organization is evident in layer 1, but the overall stratification pattern is similar to that in wild-type rat. *E-L,* Coronal (*E-G*) and tangential (through middle stratum, *I-K*) sections reacted for OCAM and VGluT2 from *SRK*. An OCAM^{+} matrix prominently surrounds OCAM^{-} patches in the middle one-third of the cortical thickness in the *SRK* (*E*). Patches of dense VGluT2-ir are also distinct and seem to correspond to the OCAM^{-} patches (*F*). Double labeling for OCAM and VGluT2 confirms that OCAM is complementary to VGluT2 (*G, K*). A similar result holds for *reeler* mice (*H, L*). Scale bar, *A-C, E-G*, 300 μm; *D, H, L*, 150 μm; *I-K*, 600 μm; insets of *A-C*, 200 μm.

In both *reeler* and *SRK*, OCAM immunohistochemistry showed a distinctly different configuration from the GRS of wild-type rodents. Instead of a laminar pattern, OCAM^{-} patches appeared within an OCAM^{+} matrix. The OCAM^{+} matrix was localized to the outer (pial) and inner (white matter) cortical zones, and surrounded OCAM^{-} patches, which were situated in the middle of the cortical thickness (Fig. 2*E, H, I* and L, and Fig. 3*E* and *H*). This is the same middle zone that contains small-cell aggregations (Fig. 1*B* and *D*); and alternate sections for Nissl and OCAM show that the cell aggregations correspond with the OCAM^{-} patches (data not shown). The aggregations and patches are comparable in shape and size, with a center-to-center distance of 50 - 150 μm in *SRK* and 40 - 100 μm in *reeler* mouse.

In both *reeler* and *SRK*, double labeling for OCAM and either VGluT1 or VGluT2 showed an orderly relationship; namely, OCAM^{-} patches matched with patches that are VGluT2^{+} (Fig. *2E-L*) and VGluT1^{-} (Fig. *3E-H*). Thus, although the normal lamination was disrupted in the mutant rodents, VGluT2 and VGluT1 have the same complementary relationship as in the wild-type, and the same association with OCAM (Table 1).
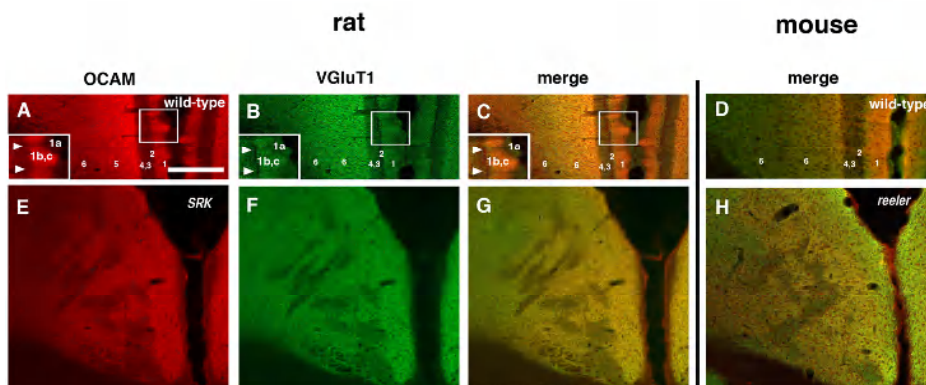

Figure 3. Architectonics of wild-type and mutant GRS, visualized by OCAM and VGluT1 (presumed to correspond to corticocortical terminals). *A-D,* Coronal sections reacted for OCAM and VGluT1 from wild-type rat (*A-C*) and wild-type mouse (*D;* merged image only). As in Figure 2, OCAM-ir in the wild-type rat (*A*) is bistratified, with a dense band in layer 1b, c and another in layers 5, 6. Note notch-like appearance in layer 1 (arrowheads in inset in *A*). VGluT1 shows a pattern similar to OCAM (*B*). Double immunofluorescence for OCAM and VGluT1 directly demonstrates overlap (*C*). Insets in *A-C* are higher magnification from the white boxes. Arrowheads in insets point to corresponding locations. As for VGluT2 (Fig. 2), there is no evidence of modularity of VGluT1 in the wild-type mouse (D). *E-H,* Tangential sections reacted for OCAM and VGluT1 from *SRK* (*E-G*). An OCAM-dense matrix in *SRK* (*E*) prominently surrounds OCAM^{-} patches in the middle one-third of the cortical thickness. A matrix of dense VGluT1-ir is also conspicuous and seems to correspond to the OCAM^{+} matrix (*F*). Double labeling for OCAM and VGluT1 confirms that OCAM colocalizes with VGluT1 (*G*). A similar result holds for *reeler* mice (*H*). Scale bar, *A-C, E-G,* 300 μm; *D, H* 150 μm; insets of *A-C,* 200 μm.

To confirm the complementary relationship of VGluT1 and 2, we further tested with AChE histochemistry, known to correspond to thalamocortical terminations from the anterior thalamic nuclei (Vogt, 1985) and with Zn histochemistry, known to correspond to a subpopulation of corticocortical terminations (Garrett et al., 1992; Casanovas-Aguilar et al., 1998; see also Fig. *4E-G*). As expected, double labeling with VGluT2 resulted in a match with AChE (Fig. 4*A, B*), but an interdigitation with Zn in the mutants (Fig. 4*C, D*), as in the wild-type rodents (Fig. 4*E-G*, Table 1).
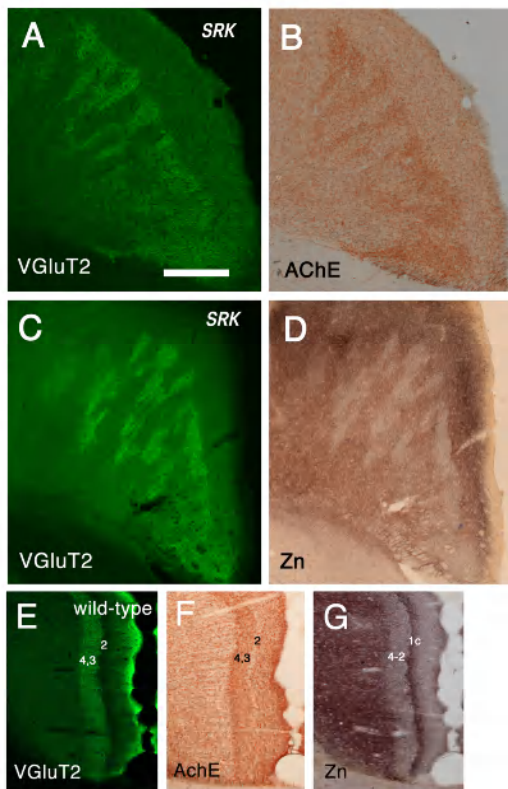
16

Figure 4. Architectonics of wild-type and mutant rat GRS, visualized in coronal sections by VGluT2, AChE and Zn. *A, B,* Single section from *SRK* reacted for VGluT2 and AChE. VGluT2-ir patches (*A*) co-localize with zones of high AChE activity (*B*). *C, D,* Single section from *SRK* reacted for VGluT2 and Zn. VGluT2-ir patches (*C*) correspond to zones low in Zn (*D*). *E, F, G,* Single section reacted for VGluT2 (*E*) and Zn (*G*) and an adjacent section reacted for AchE (*F*). A similar distribution occurs in the wild-type rat. That is, VGluT2-dense layers (1a, 3 and 4) are also dense in AChE, but weak in Zn. In addition, note that layers 1b and 2 show low levels of all three substances. Scale bar, 300 μm.

Reeler*;YFP-H mutant mouse: subiculoretrosplenial projections form patches*

In addition to thalamic and cortical inputs, a third major input to the GRS is from the subiculum (Vogt, 1985, van Groen and Wyss, 2003). To determine how this input re-organizes in the mutant GRS, we compared subicular-GRS projections in *reeler* and in the wild-type YFP-H transgenic mouse, where YFP is expressed in some neurons under the control of the promotor/enhancer of Thy-1 gene (Feng et al., 2000). In the GRS of the YFP-H mouse, YFP[+] axons form a dense band in layers 3 and 4 (Fig. 5*A-C*, Table 1). These are thalamorecipient layers, as shown by VGluT2-ir, but also receive dense subicular input (Vogt, 1985; Van Groen and Wyss, 2003). To identify the source of the YFP[+] axons, we injected ibotenic acid into the ipsilateral subiculum. Subsequent to this, the dense axon band disappeared unilateral to the lesion. There was no obvious change in either the layer 5 axonal plexus, nor VGluT2-ir (Fig. 5*D-F*); but YFP labeling in layer 1b,c is also diminished. These results suggest that the YFP[+] axons in layers 3 and 4 as well as those in 1b,c are

17

mainly of subicular origin. Consistent with this conclusion, in the YFP-H mouse, the thalamic nuclei projecting to the GRS (i.e., AV, AD and LD, Van Groen and Wyss, 2003) have very few YFP-expressing neurons, whereas most of the pyramidal neurons in the subiculum strongly express YFP (not shown).

In *reeler*; YFP-H mutant mouse, YFP axons formed patches in the GRS (Fig. 5*G-L*). These have the same appearance and size as patches positive for VGluT2 and negative for OCAM in the *reeler.* From the results in wild-type YFP-H mouse after ibotenic acid injections, these axons are likely to originate from the subiculum in the mutant as well (Table 1).
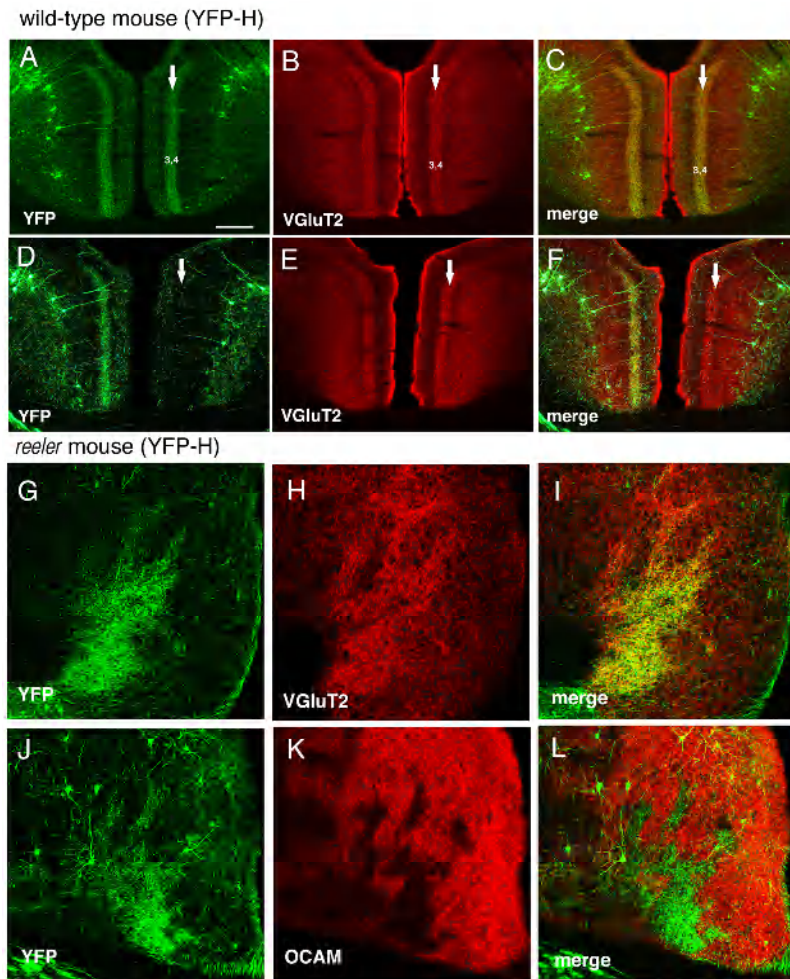
Figure 5. YFP dense terminations in the GRS of YFP-H mouse (in middle layers) and *reeler*;YFP-H mutant mice (in patches). *A-C*, Coronal section from YFP-H mouse, reacted for VGluT2. YFP[+] terminations are particularly dense in layers 3 and 4 (arrow in *A*). A similarly dense band of VGluT2-ir occurs in layers 3 and 4 (arrow in *B*). The merged image directly demonstrates the co-localization of these YFP[+] and VGluT2-ir terminations (*C*). *D-F,* Coronal section from YFP-H mouse reacted for VGluT2-ir after an ibotenic acid lesion of the subiculum. The YFP dense band has disappeared unilateral to the lesion (arrow in *D*). Labeling in layer 1b, c has also been lost, but there are no obvious changes in the layer 5 axonal plexus. VGluT2-ir remains (*E*). *G-L,* Coronal sections of *reeler*;YFP-H mutant mouse stained for VGluT2 (*H*) or OCAM (*K*). YFP[+] terminatins form patches, which closely overlap with VGluT2-ir patches (*G-I*) and fill OCAM[-] patches (*J-L*). Scale bar, 300 μm.

Generality of patch-matrix-like organization in other cortical areas of mutant rodents

Although this investigation is concentrated on the GRS, OCAM immunohistochemistry revealed a patch and matrix configuration widely throughout the cerebral hemisphere, in visual, auditory, barrel, perirhinal, and anterior cingulate cortical areas (Fig. 6). The expression level tended to be lower than that in the GRS, and there was some area-specific variability in the shape of the patch compartments and their position within the cortical thickness. Further detail and additional results will be described in a separate communication (Wintzer, Ichinohe, Yoshihara, Ogawa and Rockland, in preparation).
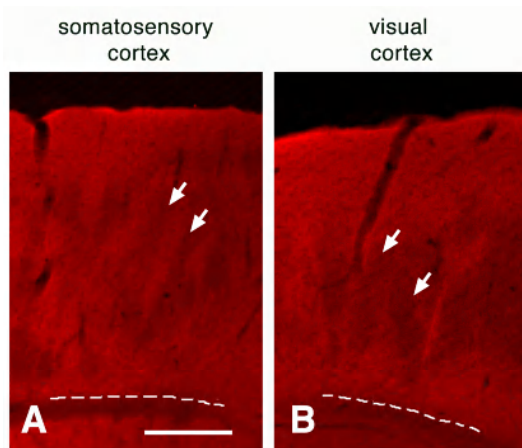

Figure 6. Patch-matrix-like organization in two coronal sections through barrel (A) and visual (B) cortices in *reeler* mouse, visualized by OCAM immunohistochemistry. An OCAM⁺ matrix prominently surrounds OCAM⁻ patches (arrows) in the middle one-third of the cortical thickness in both areas. Broken lines are borders of gray and white matter. Scale bar, 300 μm.

Postsynaptic localization of OCAM-ir in wild-type and mutant rodent GRS

In a previous EM study of layers 1-4 of wild-type rat GRS, we reported that OCAM-ir structures are largely dendritic, and that these originate from layer 5 neurons (Ichinohe et al., 2003). To establish the identity in mutant rodent, we first compared *in situ* hybridization in wild-type and mutant. OCAM mRNA in GRS of wild-type mouse was strongly expressed in layer 5 neurons as expected, with moderate expression as well in layer 6, but no signal was apparent in supragranular neurons (Fig. 7*A*, Table 1). In the *reeler* GRS, OCAM mRNA expression was found throughout the cortical thickness. This is consistent with previous descriptions that connectionally defined layer 5 pyramidal neurons are radially scattered (Fig. 7*B*; Terashima et al., 1983; Hoffarth et al., 1995; Polleux et al., 1998: Baba et al., 2007). In

the immediate subpial zone, presumed to correspond mainly to an inverted layer 6 (Aoki et al., 2002; Yamamoto et al., 2003), many neurons expressed OCAM mRNA. Deeper, patch-like areas (Arrows in Fig. *7C*) contained fewer OCAM mRNA expressing neurons; and by comparison with an adjacent section, stained for OCAM protein, these patches could be ascertained to match with OCAM⁻ patches (Arrows in Fig. 7*C,D*, Table 1). From these results, we conclude that OCAM-ir dendrites in *reeler* GRS likely originate from displaced layer 5 pyramidal neurons.
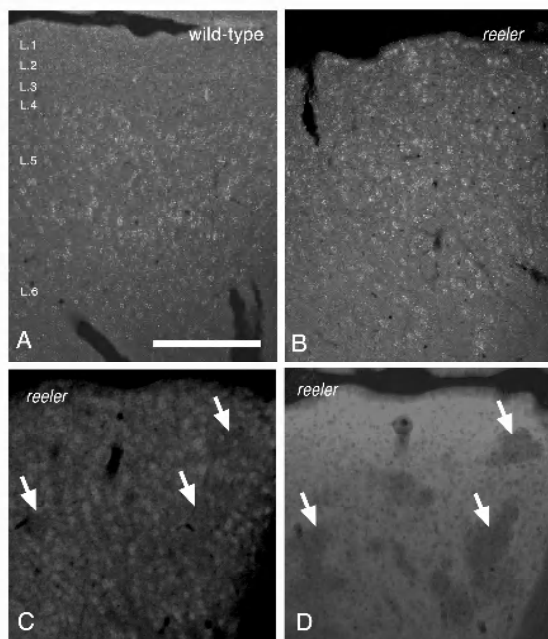
Figure 7. OCAM mRNA signals are confined to infragranular layers in wild-type mouse, but are scattered throughout the cortical thickness in *reeler* mouse. *A, B,* Coronal sections stained for OCAM mRNA by *In situ* hybridization in wild-type mouse (*A*) and *reeler* mouse (*B*). *C, D,* Adjacent *reeler* coronal sections stained by *in situ* hybridization (*C*) and immunohistochemistry (*D*) for OCAM mRNA and protein, respectively. Patch-like areas containing fewer OCAM mRNA expressing neurons were evident (arrows in *C*), which seem to match with OCAM⁻ patches (arrows in *D*). Scale bar, *A,B,* 300 μm; *C,D,* 150 μm.

Next, we carried out EM investigations of OCAM-ir structures in the mutant rodents. As expected, in both *reeler* mice and *SRK*, the majority of OCAM-ir structures (in OCAM$^+$ matrix) were dendritic. These could be identified as spines and small-caliber dendrites (< 1 μm; about 90% of all OCAM-ir structures) as well as large caliber dendrites (> 1 μm; about 10% of all OCAM-ir structures). OCAM-ir somata were evident, but OCAM$^+$ axons or synapses were rare, as in the wild-type (< 1% of profiles examined). For somata, the external cell membrane and endoplasmic reticulum were immunoreactive (Fig. 8*A, B*). OCAM-ir dendrites can frequently be seen in direct dendrite-dendrite apposition and sometimes in soma-dendritic apposition. However, there was no indication of junctional

specializations (*e.g.*, gap junctions) (Fig. 8*A, C-E*), nor of simultaneously labeled pre- and postsynaptic elements. Similar results were obtained from layer 5 of the wild-type rodents (data not shown; for layers 1-4 see also Ichinohe et al., 2003).
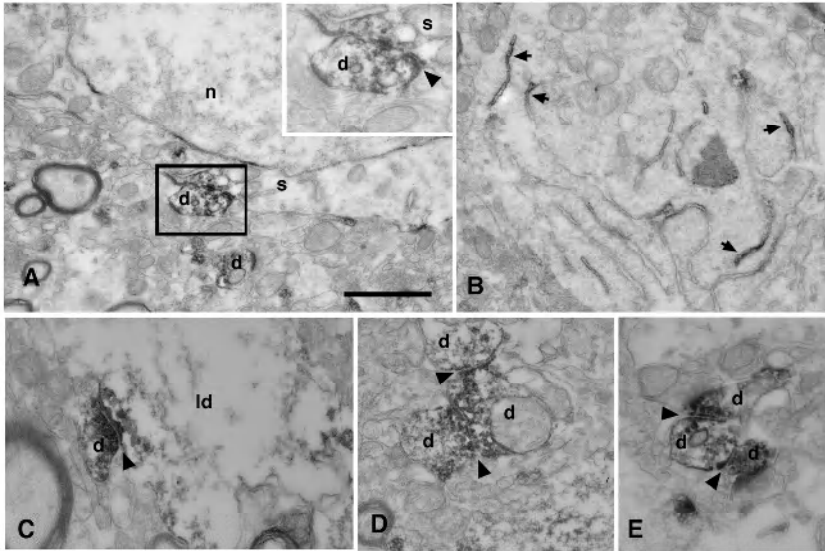

Figure 8. Electron microscopy shows that, in the wild-type and mutant GRS, OCAM-ir structures are mainly somata and dendrites, and these are frequently in close apposition. *A-E*, Electron micrographs of OCAM-ir structures from the OCAM$^+$ matrix in the middle stratum of *SRK*. An OCAM-ir small dendrite (d) and soma (s) are closely apposed (arrowhead in inset *A*); Close contacts between small and large dendrites (ld)(arrowhead in *C*) and among a group of three small dendrites (arrowheads in *D, E*). Portions of the endoplasmic reticulum (arrows in *B*) within somata are also OCAM-ir. Abbreviation: n, nuclelus. Scale bar, *A, B*, 2 μm; *C-E,* inset in *A*, 1.2 μm.

In samples from an OCAM$^-$ patch, we could find some OCAM-ir somata and dendrites (data not shown), as predictable from the *in situ* hybridization data (Table 1). However, OCAM-ir structures were considerably fewer than in the OCAM$^+$ matrix, consistent with light microscopic observations. The level of OCAM-ir is presumed to correlate with the degree of dendritic branching of OCAM$^+$ layer 5 neurons. In wild-type rodents, apical dendrites passing through layer 2-4 in wild-type rodents appear as OCAM$^+$ profiles (see Fig. 5 in Ichinohe et al., 2003). Subpopulations of layer 5 neurons with abundant branches in OCAM$^-$ layer 2-4 (see Fig. 5 in Wyss et al., 1990) are assumed to be OCAM$^-$.

Dendritic arbors prefer specific OCAM compartments

Our next question was whether the malpositioned dendrites in *reeler* and *SRK* would have any orderly relationship to the OCAM-delineated patch or matrix. We addressed this issue

by visualizing single dendritic arbors (filled by Lucifer Yellow injection in fixed slice) in relation to OCAM-ir. The results were compared between wild-type and *reeler* mice.

In wild-type mice, we filled and reconstructed 7 neurons in layers 2 and upper 3, and 11 neurons in layer 5. Six of the 7 supragranular neurons clearly elaborated dendrites in OCAM⁻ layers (i.e., layer 1a, and 2-4, Fig. 9*A, B*). That is, apical dendrites of these supragranular neurons branched extensively in layer 1a (OCAM⁻), but not layer 1b, c; and their basal dendrites rarely entered layer 1b, c or layer 5 (OCAM⁺). In contrast, all of the 11 infragranular neurons elaborated dendrites in OCAM⁺ layers (i.e., layer 1b,c, and layer 5, Fig. 9*C*). Some of their basal and oblique dendrites ascended upward toward the pia, but rarely invaded layer 4 (OCAM⁻).
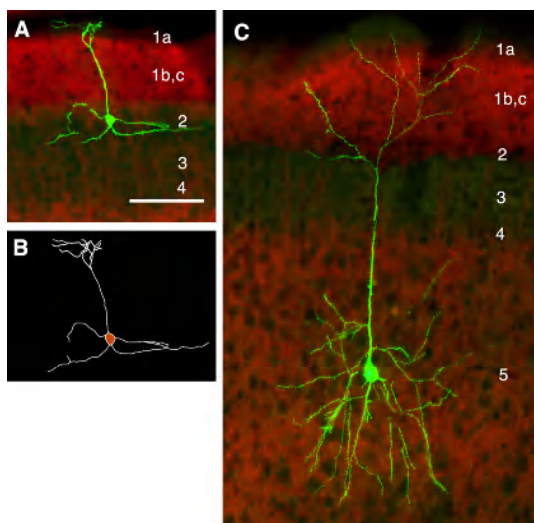

Figure 9. Pyramidal cells in GRS of wild-type mouse have soma/dendritic preferences for either OCAM⁺ or OCAM⁻ layers. *A,* Coronal section with a LY-filled neuron (green), reacted for OCAM (red). This layer 2 neuron has soma, apical tuft, and basal dendrites in OCAM⁻ layers (i.e., layer 1a, and 2-4). *B,* Reconstruction and flattened image of the neuron in *A. C,* Coronal section with a LY-filled neuron (green), reacted for OCAM (red). This layer 5 neuron has soma, apical tuft, and basal dendrites in OCAM⁺ layers (i.e., layer 1b,c, and layer 5). Scale bar, 50 μm.

In *reeler*, large layer 5 neurons (putative OCAM⁺) are dispersed and their normal dendritic orientation is in general lost (Terashima et al., 1992). Despite these anomalies, we were able to ascertain a strong tendency for either dendritic preference or avoidance of specific OCAM compartments. Of 17 neurons filled and reconstructed, 10 arbors were preferentially within the OCAM⁺ matrix and 7 were preferentially within the OCAM⁻ patch (Fig. 10). Of the 10 neurons with dendrites preferring the OCAM⁺ matrix, for 8 the somata

were also within the OCAM$^+$ matrix (Table 2). The 2 other neurons are likely to be displaced

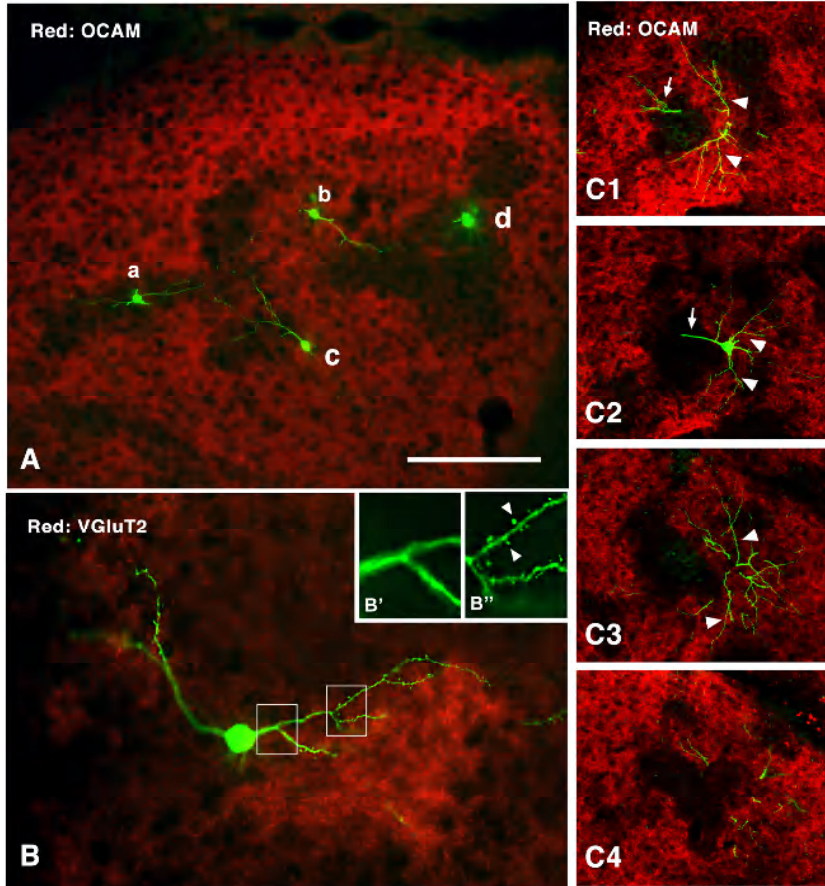layer 5 cells (see *in situ* hybiridization for OCAM, Fig. 7).

Figure 10. Pyramidal cell dendrites preferentially arborize in either patch or matrix compartments in *reeler* GRS. *A,* Coronal section reacted for OCAM (red), with four LY-filled neurons (green). Somata of two neurons (**a** and **d**) are located in OCAM$^-$ patches, and their dendrites stay within OCAM$^-$ patches. Two other neurons (**b** and **c**) are located in the OCAM$^+$ matrix, but their dendrites elaborate branches in an OCAM$^-$ patch. *B,* Coronal section reacted for LY (green) and VGluT2 (red). A LY-filled neuron has soma located in a zone of low VGluT2-ir (presumably equivalent to the OCAM$^+$ matrix). Dendrites branch within a VGluT2-dense patch (presumably equivalent to a OCAM$^-$ patch). These dendritic portions have spines (arrowheads in *B''*), but not the portions outside the VGluT2-dense region (*B'*). Insets in *B* (i.e., *B', B''*) are higher magnification from the white boxes (B' from left box, B'' from right box). *C1-C4,* Serial sections of a LY-filled neuron, double-reacted for OCAM. The cell body is located within the OCAM$^+$ matrix (*C2*). An apical dendrite-like process gives off an oblique dendrite proximally, before entering an OCAM$^-$ patch. An apical tuft branches just at the border between patch and matrix compartments (arrow in *C1*). The basal dendrites tend, like the cell body, to stay within the OCAM$^+$ matrix. Scale bar, *A, C1-C4,* 100 μm: *B,* 50 μm; *B', B''*, 20 μm.

For the sake of an objective classification, we calculated a ratio to express the

length of dendrite in the matrix compartment in relation to total dendritic length (matrix/total

dendritic length or "M/T ratio," Table 2). An M/T histogram (Fig. 11*A*), based on

reconstructions of the 17 filled neurons, reveals two groups, *i.e.*, one is below 0.2 and the

other is above 0.5. We defined neurons with a number below 0.5 as patch-preferring neuron

(n = 7), and those with an M/T number greater than 0.5 as matrix-preferring neuron (n = 10;

Table 2 dotted line). The resultant grouping agrees with the more qualitative classifications described above.

Table 2. Dendritic matrix/total ratio of original (0 degree) and three turned positions of *reeler* mouse

Cell number	total dendrite length	matrix/total ratio of dendrites				cell body localization
		0 degree	90 degree	180 degree	270 degree	
#1	3197	**0.000**	**0.020**	**0.024**	**0.179**	patch
#2	501	**0.052**	**0.558**	**0.080**	**0.280**	matrix
#3*	603	**0.062**	**0.534**	**0.217**	**0.373**	patch
#4*	1127	**0.087**	**0.435**	**0.598**	**0.637**	patch
#5*	1773	**0.112**	**0.251**	**0.359**	**0.184**	matrix
#6	1262	**0.117**	**0.417**	**0.505**	**0.450**	patch
#7	2453	**0.176**	**0.533**	**0.458**	**0.386**	matrix
#8	905	**0.563**	**0.337**	**0.202**	**0.405**	patch
#9	1553	**0.622**	**0.475**	**0.698**	**0.585**	matrix
#10	967	**0.673**	**0.274**	**0.252**	**0.123**	patch
#11	1853	**0.764**	**0.361**	**0.477**	**0.439**	matrix
#12	787	**0.842**	**0.513**	**0.447**	**0.464**	matrix
#13*	4392	**0.851**	**0.588**	**0.523**	**0.569**	matrix
#14	1855	**0.879**	**0.550**	**0.483**	**0.808**	matrix
#15	610	**0.884**	**0.804**	**0.700**	**0.700**	matrix
#16	1483	**0.888**	**0.801**	**0.807**	**0.696**	matrix
#17	1835	**0.978**	**0.957**	**0.805**	**0.879**	matrix

*#3 is cell **a** in Fig. 10*A*, #4 is cell **d** in Fig. 10*A*, #5 is cell **b** in Fig. 10*A*, #7 is cell **c** of Fi.g 10*A*, #13 is cell in Fig 10*C1-C4*.

¶Neurons above dotted line are patch-preferring (M/T ratio in 0 degree position < 0.2), and neurons below are matrix-preferring (M/T ratio in 0 degree position > 0.5). See **Materials and Methods**, and **Results**.
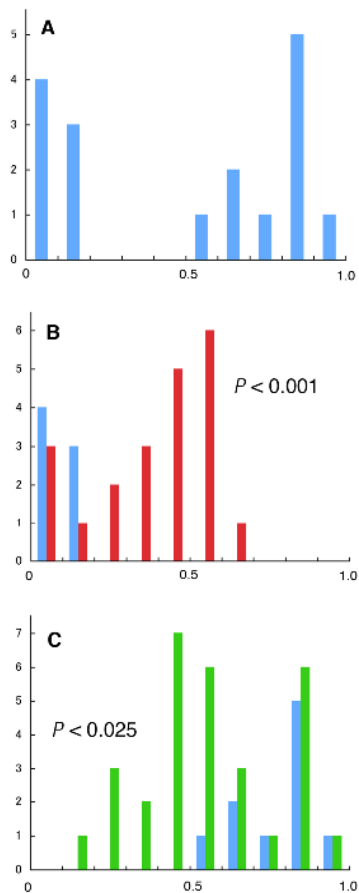
Figure 11. Quantitative M/T ratio analysis (dendritic length in OCAM[+] matrix (M) divided by total length of dendrites (T)), for 17 reconstructed LY-filled neurons. *A,* Histogram of dendritic M/T ratio of all 17 reconstructed neurons. Note that there are two peaks (<0.5; >0.5), corresponding to two separable populations. *B,* Histogram of M/T ratio of 7 patch preferring neurons (M/T ratio < 0.5: blue bar), and M/T ratio of the same cells re-calculated after rotating the dendrites around the cell body by 90, 180, 270 degree (red bars). The M/T ratios for the original position are, in general, smaller than those in the rotated positions. The difference is statistically significant ($P < 0.001$). *C,* Histogram of M/T ratio of 11 matrix preferring neurons (M/T ratio > 0.5: blue bar), and M/T ratio of the same cells re-calculated after rotating the dendrites around the cell body, by 90, 180, 270 degrees (green bar). The M/T ratios for the original position are, in general, larger than those in the rotated positions. The difference is statistically significant ($P < 0.025$).

Since the length of dendrite within a patch may be strongly influenced by the 3-dimensional configuration of the surrounding patch and matrix, we have attempted to compensate for this by computer-rotation of the reconstructed dendrites while holding constant the position of the cell body. 90, 180, and 270 degree rotations were carried out against a fixed patch-matrix configuration (Fig. S1), and the M/T ratio was re-calculated for these three conditions (Table 2, Fig. 11*B, C*). The 0 degree position (original position: blue column) is obviously skewed to either a low or high M/T number compared to the three rotated positions (90, 180, 270 degree: red column in Fig. 11*B* for patch-preferring neurons, and green column in Fig. 11*C* for matrix-preferring neurons). The Kruskal-Wallis test shows that this deviation is statistically significant ($P < 0.001$ for patch-preferring neurons, and $P < 0.025$ for matrix-preferring neurons). This supports our interpretation that the position of the cell body is less important than the active preference of dendrites for either patch or matrix domain.

25

DISCUSSION

In the GRS of wild-type rodents, thalamocortical (VGluT2) and corticocortical (VGluT1) inputs are highly stratified, with a complementary relationship to each other.   Layers 1a, 3, and 4 are positive for VGluT2 and layers 1b,c and 5 are positive for VGluT1. In layer 1b, the two systems form a small-scale modular organization in relation to apical dendrites of layer 2 neurons (co-localized with VGluT2) and distal tufts of layer 5 neurons (co-localized with VGluT1). This organization is also discernible with immunohistochemistry for OCAM, a cell adhesion molecule associated mainly with dendrites of layer 5 neurons, where OCAM-ir corresponds to corticocortical layers and modules.

In this study, the use of OCAM as reference marker revealed a distinct patch and matrix configuration in the GRS of both *reeler* and *SRK* mutants, where thalamocortical and corticocortical inputs maintain the same complementary relationship as in the wild-type rodents (respectively corresponding to OCAM$^-$ patches and an OCAM$^+$ matrix). The patch and matrix mosaic is particularly evident in the GRS, but a recognizably similar organization can be discerned widely throughout the cortex (Fig. 6 and Wintzer, Ichinohe, Yoshihara, Ogawa and Rockland, in preparation).

Segregation of inputs, by modules or layers, is a basic cortical feature; and modular segregation occurs as well in other structures, such as the superior colliculus (Mana and Chevalier, 2001) and striatum (Joel and Weiner, 2001). In some areas, notably the primary sensory, input segregation is associated with parallel submodality (e.g., rodent barrel cortex; Chmielowska et al., 1989: monkey visual cortex; Casagrande and Kaas, 1994). In the nigro-collicular pathway, modularity is proposed as working to select motor programs for different classes of orienting behavior (Mana and Chevalier, 2001). In the GRS, the coincidence of subicular and thalamocortical inputs suggests a convergence and interaction of place (subicular) and head-direction (thalamic) properties (Smith and Mizumori, 2006; Taube, 2007). A specialized cell type, head-direction dependent place cell, so far unique to

the GRS, may require combination of these inputs (Cho and Sharp, 2001).

Early investigations of thalamocortical terminations to sensory cortex show an elongated patchy distribution (Caviness and Frost, 1983), reminiscent of the VGluT2$^+$/OCAM$^-$ patches in our material. Dispersed thalamocortical aggregates can also be detected by cytochrome oxidase in *reeler* and *SRK* somatosensory cortex (for *reeler*, Fig. 4 in Strazielle et al., 2006; for *SRK*, Higashi et al., 2005).

One previous study of *reeler* mouse demonstrated a striking mosaic of AChE$^+$ and AChE$^-$ zones (Steindler et al., 1994), which seems identical to our results. In that study, the mosaic was assigned to visual cortex; but in retrospect, it may actually have been in the GRS. That is, in our material, the density of AChE activity abruptly declines at the lateral edge of GRS (unpublished observation, and see Fig. 4*B*).

So far, there has been little evidence from retrograde labeling experiments in other areas of any patch-matrix organization. Corticothalamically projecting neurons are displaced superficially, in a bandlike pattern (Aoki et al., 2002; Yamamoto et al., 2003). Callosally projecting neurons are abnormally biased to the deeper two-thirds (Caviness and Yorke, 1976; Terashima et al., 1985; Aoki et al., 2002). Layer 5 corticospinal neurons are abnormally biased to the upper cortical stratum, but are more precisely described as radially scattered (motor cortex; Terashima et al., 1983; Hoffarth et al., 1995; Polleux et al., 1998: sensory-motor cortex, Ikeda and Terashima, 1997: areas 3 and 6; Polleux et al., 1998). Similarly, layer 5 corticotectal neurons in the visual cortex are widely scattered from the white matter to the pial surface (Baba et al., 2007). However, in one report, where young *reeler* mice received injections to visualize corticobrainstem, corticospinal and

corticothalamic neurons in somatic sensorimotor cortex (injection: P2; perfusion: P5), there is some indication of cell-sparse patches (OCAM$^-$?) in the middle of a cell-filled "matrix" (Fig. 1 in Hoffarth et al., 1995). The apparent absence of conspicuous patchiness of projection neurons most likely can be attributed to differences in dendritic vs. soma location.

Dendrite-dendrite interaction and a role for OCAM

We are proposing that the patch-matrix mosaic results in part from dendrite-dendrite interactions, where the OCAM$^+$ dendrites of a subgroup of layer 5 neurons (see **RESULTS**: ***Postsynaptic localization of OCAM-ir in wild-type and mutant rodent GRS***) aggregate to form the matrix compartment by homophilic interactions, and influence patch formation by heterophilic repulsion. This is the mechanism proposed for the formation of dendritic modules in the uppermost layers in the wild-type rat (Ichinohe et al., 2003). In support of this proposal, *in situ* hybridization in the mutant rodents revealed that neurons that highly express OCAM mRNA (putative layer 5 neurons) tend to avoid OCAM- patches. In addition, dendritic arbors, visualized by filling with Lucifer Yellow, appear to selectively sample from compartments that are OCAM$^-$ (dendrites of layer 2 neurons) or OCAM$^+$ (dendrites of layer 5 neurons; Fig. 9).

Clearly, the establishment of lamination (wild-type) or compartments (mutants) involves multiple mechanisms. At early stages (E15-E17), afferent systems (i.e., monoaminergic fibers) have been proposed as an important determinant of the direction of dendritic growth (Pinto Lord and Caviness, 1979), and in barrel cortex, the influence of thalamocortical connections on dendritic orientation of stellate cell is well-established (Harris and Woolsey, 1979; Steffen and Van der Loos, 1980; Datwani et al., 2002). Our proposal, that dendrite-dendrite interactions are another important factor at the early postnatal stages, might be further investigated by selective lesioning of the thalamocortical or other inputs (for

serotonergic inputs and presubiculum, see Janusonis et al., 2004), with the prediction that the basic patch-matrix will persist.

In layer 1 of the wild-type GRS, modularity is apparent with dendritic markers from as early as P3 by OCAM (or P5 by GluR2/3; Ichinohe et al., 2003), but according to Ma et al. (2002), thalamocortical axons have just reached the subplate of the GRS at P3. If additional experiments confirmed a similar early time course of OCAM expression in the *reeler* and *SRK*, this would provide further support for an instructive role for dendrites in the formation of the patch-matrix mosaic. The time of arrival for subicular afferents is not known.

Both dendrite-dendrite and dendrite-axon interactions have been extensively investigated in the context of dendritic field formation, maintenance, and remodeling, and are well-known to involve multiple cellular and molecular mechanisms (Datwani et al., 2002; Wong and Ghosh, 2002; Lardi-Studler and Fritschy, 2007; Parrish et al., 2007). Undoubtedly, therefore, the proposed homophilic-heterophilic dendritic influences of OCAM in the GRS are one of multiple signaling mechanisms.

The role of OCAM has been intensively investigated in the olfactory system of mice (Yoshihara et al., 1997; Alenius and Bohm, 1997; von Campenhausen et al., 1997; Nagao et al., 2000; Treloar et al., 2003; Hamlin et al., 2004; Waltz et al., 2006). It is known to be expressed in axons of a subset of sensory neurons in the ventral olfactory epithelium (which target OCAM$^-$ dendrites), and in dendrites of dorsally located neurons in the olfactory bulb (which receive OCAM$^-$ axons; Treloar et al., 2003). These complementary expressions have recently been implicated in the intraglomerular compartmentalization, which is disrupted in OCAM-deficient mice (Waltz et al., 2006). In the GRS, there is a preponderant

association of OCAM with postsynaptic dendrites, not axons, which is why we have proposed a mechanism of population-dependent dendritic attraction or repulsion (Ichinohe et al., 2003; this study). It seems clear that OCAM can influence modular formation in a range of different environments (wild-type GRS, mutant GRS, and olfactory bulb).

In summary, we have demonstrated a patch-matrix mosaic in the *reeler* mutants, and proposed that this is in part based on segregation of specific inputs in relation to subpopulations of dendrites. Similar methods, using OCAM, VGluT1, and VGluT2 as a reference markers, may be applicable for investigating input-target relationships in transgenic mice with defects in cellular migration and positioning, morphology of pyramidal cell dendrites, or afferent ingrowth (e.g., cGMP-dependent protein kinase I knockout mouse, doublecortin knockout mouse, Cdk5 knockout mouse: Demyanenko et al., 2005; Deuel et al., 2006; Ohshima et al., 2007).

Supplementary Material

Supplementary material can be found at : http://www.cercor.oxfordjournals.org/.
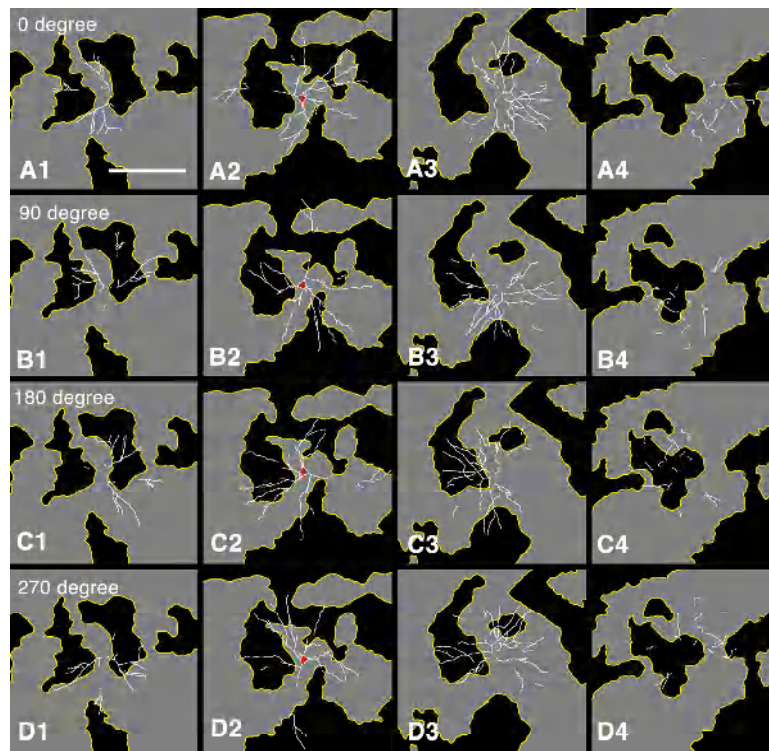
Notes

30

Figure S1

References

Aikawa H, Nonaka I, Woo M, Tsugane T, Esaki K. 1988. Shaking rat Kawasaki (*SRK*): a new neurological mutant rat in the Wistar strain. Acta Neuropathol (Berl). 76:366-372.

Agmon A, Yang LT, O'Dowd DK, Jones EG. 1993. Organized growth of thalamocortical axons from the deep tier of terminations into layer IV of developing mouse barrel cortex. J Neurosci. 13:5365-5382.

Alenius M, Bohm S. 1997. Identification of a novel neural cell adhesion molecule-related gene with a potential role in selective axonal projection. J. Biol. Chem. 272:26083–26086.

Aoki T, Matsunaga T, Misaki K, Watanabe Y, Terashima T. 2002. Abnormal distributions of callosal commissural and corticothalamic neurons in the cerebral neocortex of Shaking Rat Kawasaki. Neuroscience. 114:427-438.

Baba K, Sakakibara S, Setsu T, Terashima T. 2007. The superficial layers of the superior colliculus are cytoarchitectually and myeloarchitectually disorganized in the reelin-deficient mouse, reeler. Brain Res. 1140:205-215.

Casagrande VA, Kaas JH. 1994. The afferent, intrinsic, and efferent connections of primary visual cortex in primates. In: Peters A, Rockland KS, editors. Cerebral Cortex Vol. 10. New York: Plenum. p 201–259.

Casanovas-Aguilar C, Reblet C, Perez-Clausell J, Bueno-Lopez JL. 1998. Zinc-rich afferents to the rat neocortex: projections to the visual cortex traced with intracerebral selenite injections. J Chem Neuroanat. 15:97–109

Caviness VS Jr, Rakic P. 1978. Mechanisms of cortical development: a view from mutations in mice. Annu Rev Neurosci. 1:297-326.

Caviness VS Jr, Frost DO. 1983. Thalamocortical projections in the reeler mutant mouse. J Comp Neurol. 219:182-202.

Caviness VS Jr, Yorke CH. 1976. Interhemispheric neocortical connections of the corpus callosum in the reeler mutant mouse: a study based on anterograde and retrograde

methods. J Comp Neurol. 170:449-459.

Caviness VS, Crandall JE, Edwards MA. 1988. The reeler malformation: implications for neocortical histogenesis. In: Peters A, Jones EG, editors. Cerebral Cortex Vol. 5. New York: Plenum, 1988, vol. 7, p. 58-89.

Chmielowska J, Carvell GE, Simons DJ. 1989. Spatial organization of thalamocortical and corticothalamic projection systems in the rat SmI barrel cortex. J Comp Neurol. 285:325-338.

Cho J, Sharp PE. 2001. Head direction, place, and movement correlates for cells in the rat retrosplenial cortex. Behav Neurosci. 115:3-25.

D'Arcangero G, Nakajima K, Miyata T, Ogawa M, Mikoshiba K, Curran T. 1997 Reelin is a secreted glycoprotein recognized by the CR-50 monoclonal antibody. J Neurosci. 17: 23-31.

Datwani A, Iwasato T, Itohara S, Erzurumlu RS. 2002. NMDA receptor-dependent pattern transfer from afferents to postsynaptic cells and dendritic differentiation in the barrel cortex. Mol Cell Neurosci. 21:477-492.

Demyanenko GP, Halberstadt AI, Pryzwansky KB, Werner C, Hofmann F, Maness PF. 2005. Abnormal neocortical development in mice lacking cGMP-dependent protein kinase I. Brain Res Dev Brain Res. 160:1-8.

Deuel TA, Liu JS, Corbo JC, Yoo SY, Rorke-Adams LB, Walsh CA. 2006. Genetic interactions between doublecortin and doublecortin-like kinase in neuronal migration and axon outgrowth. Neuron. 49:41-53.

Feng G, Mellor R H, Bernstein M, Keller-Peck C, Nguyen QT, Wallace M, Nerbonne JM, Lichtman JW, Sanes JR. 2000. Imaging neuronal subsets in transgenic mice expressing multiple spectral variants of GFP. Neuron. 28:41-51.

Fujiyama F, Furuta T, Kaneko T. 2001. Immunocytochemical localization of candidates for vesicular glutamate transporters in the rat cerebral cortex. J Comp Neurol. 435:379-387.

Garrett B, Sorensen JC, Slomianka L. 1992. Fluoro-Gold tracing of zinc-containing afferent connections in the mouse visual cortices. Anat. Embryol. 185:451–459.

Hamlin JA, Fang H, Schwob JE. 2004. Differential expression of the mammalian homologue of fasciclin II during olfactory development in vivo and in vitro. J Comp Neurol. 474:438-452.

Harris RM, Woolsey TA. 1979. Morphology of Golgi-impregnated neurons in mouse cortical barrels following vibrissae damage at different post-natal ages. Brain Res. 161:143–149.

Higashi S, Hioki K, Kurotani T, Kasim N, Molnar Z. 2005. Functional thalamocortical synapse reorganization from subplate to layer IV during postnatal development in the reeler-like mutant rat (shaking rat Kawasaki). J Neurosci. 25:1395-1406.

Hof PR, Young WG, Bloom FE, Belichenko PV, Celio, MR. 2000. Comparative Cytoarchitectonic Atlas of the C57BL/6 and 129/Sv Mouse Brains. Amsterdam: Elsevier Science.

Hoffarth RM, Johnston JG, Krushel LA, van der Kooy D. 1995. The mouse mutation reeler causes increased adhesion within a subpopulation of early postmitotic cortical neurons. J Neurosci. 15:4838-4850.

Ichinohe N, Rockland KS. 2002. Parvalbumin positive dendrites co-localize with apical dendritic bundles in rat retrosplenial cortex. Neuroreport. 13, 757-761.

Ichinohe N, Yoshihara Y, Hashikawa T, Rockland KS. 2003. Developmental study of dendritic bundles in layer 1 of the rat granular retrosplenial cortex with special reference to a cell adhesion molecule, OCAM. Eur. J. Neurosci. 18: 1764-1774

Ikeda Y, Terashima T. 1997. Corticospinal tract neurons are radially malpositioned in the sensory-motor cortex of the Shaking rat Kawasaki. J Comp Neurol. 383:370-380.

Janusonis S, Gluncic V, Rakic P. 2004. Early serotonergic projections to Cajal-Retzius cells: relevance for cortical development. J Neurosci. 24:1652-1659.

Joel D, Weiner I. 2000. The connections of the dopaminergic system with the striatum in rats and primates: an analysis with respect to the functional and compartmental organization of the striatum. Neuroscience. 96:451-474.

Kaneko T, Fujiyama F, Hioki H. 2002. Immunohistochemical localization of candidates for

vesicular glutamate transporters in the rat brain. J Comp Neurol. 444:39-62.

Kikkawa S, Yamamoto T, Misaki K, Ikeda Y, Okado H, Ogawa M, Woodhams PL, Terashima T. 2003. Missplicing resulting from a short deletion in the reelin gene causes reeler-like neuronal disorders in the mutant shaking rat Kawasaki. J Comp Neurol. 463:303-315.

Lambert de Rouvroit C, Goffinet AM. 1998. The reeler mouse as a model of brain development. Adv Anat Embryol Cell Biol. 150:1-106.

Landrieu P, Goffinet A. 1981. Inverted pyramidal neurons and their axons in the neocortex of reeler mutant mice. Cell Tissue Res. 218:293-301.

Lardi-Studler B, Fritschy JM. 2007. Matching of pre- and postsynaptic specializations during synaptogenesis. Neuroscientist. 13:115-126.

Ma L, Harada T, Harada C, Romero M, Hebert JM, McConnell SK, Parada LF. 2002. Neurotrophin-3 is required for appropriate establishment of thalamocortical connections. Neuron. 36:623-634.

Mana S, Chevalier G. 2001. The fine organization of nigro-collicular channels with additional observations of their relationships with acetylcholinesterase in the rat. Neuroscience. 106:357-374.

Miro-Bernie N, Ichinohe N, Perez-Clausell J, Rockland KS. 2006. Zinc-rich transient vertical modules in the rat retrosplenial cortex during postnatal development. Neuroscience. 138:523-535.

Nagao H, Yoshihara Y, Mitsui S, Fujisawa H, Mori K. 2000. Two mirror-image sensory maps with domain organization in the mouse main olfactory bulb. Neuroreport. 11:3023-3027.

Ohshima T, Hirasawa M, Tabata H, Mutoh T, Adachi T, Suzuki H, Saruta K, Iwasato T, Itohara S, Hashimoto M, Nakajima K, Ogawa M, Kulkarni AB, Mikoshiba K. 2007. Cdk5 is required for multipolar-to-bipolar transition during radial neuronal migration and proper dendrite development of pyramidal neurons in the cerebral cortex. Development. 134:2273-2282.

Parrish JZ, Emoto K, Kim MD, Jan YN. 2007. Mechanisms That Regulate Establishment, Maintenance, and Remodeling of Dendritic Fields. Annu Rev Neurosci. *in press*.

Paxinos G, Watson C. 2004. The Rat Brain in Stereotaxic Coordinates. Amsterdam: Elsevier Science.

Peters A, Palay S, Webster H. 1991. The fine structure of the nervous system: neurons and their supporting cells. New York: Oxford University Press.

Pinto Lord MC, Caviness VS Jr. 1979. Determinants of cell shape and orientation: a comparative Golgi analysis of cell-axon interrelationships in the developing neocortex of normal and reeler mice. J Comp Neurol. 187:49-69.

Polleux F, Dehay C, Kennedy H. 1998. Neurogenesis and commitment of corticospinal neurons in reeler. J Neurosci. 18: 9910-9923.

Schlaggar BL, O'Leary DD. 1994. Early development of the somatotopic map and barrel patterning in rat somatosensory cortex. J Comp Neurol. 346:80-96.

Smith DM, Mizumori SJ. 2000. Hippocampal place cells, context, and episodic memory. Hippocampus. 16:716-729.

Steffen H, Van der Loos H. 1980. Early lesions of mouse vibrissal follicles and their influence on dendrite orientation in the cortical barrelfield. Exp. Brain Res. 40:419–431.

Steindler DA, Faissner A, Harrington KL. 1994. A unique mosaic in the visual cortex of the reeler mutant mouse. Cereb Cortex. 4:129-137.

Strazielle C, Hayzoun K, Derer M, Mariani J, Lalonde R. 2006. Regional brain variations of cytochrome oxidase activity in Relnrl-orl mutant mice. J Neurosci Res. 83:821-831.

Tabata H, Nakajima K. 2002. Neurons tend to stop migration and differentiate along the cortical internal plexiform zones in the Reelin signal-deficient mice. J Neurosci Res. 69:723-730.

Taube JS. 2007. The Head Direction Signal: Origins and Sensory-Motor Integration. Annu Rev Neurosci. *in press*.

Terashima T, Inoue K, Inoue Y, Mikoshiba K, Tsukada Y. 1983. Distribution and morphology

of corticospinal tract neurons in reeler mouse cortex by the retrograde HRP method. J Comp Neurol. 218:314-326.

Terashima T, Inoue K, Inoue Y, Mikoshiba K, Tsukada Y. 1985. Distribution and morphology of callosal commissural neurons within the motor cortex of normal and reeler mice. J Comp Neurol. 232:83-98.

Terashima T, Takayama C, Ichikawa R, Inoue Y. 1992. Dendritic arbolization of large pyramidal neurons in the motor cortex of normal and reeler mutant mouse. Okajimas Folia Anat Jpn. 68:351-363.

Treloar HB, Gabeau D, Yoshihara Y, Mori K, Greer CA. 2003. Inverse expression of olfactory cell adhesion molecule in a subset of olfactory axons and a subset of mitral/tufted cells in the developing rat main olfactory bulb. J Comp Neurol. 458:389-403.

Tsuji S. 1998. Electron microscopic localization of acetylcholinesterase activity in the central nervous system: chemical basis of a catalytic activity of Hatchett's brown (cupric ferrocyanide) precipitate revealed by 3,3'-diaminobenzidine. Folia Histochem Cytobiol. 36:67-70.

Van Groen T, Wyss JM. 2003. Connections of the retrosplenial granular b cortex in the rat. J Comp Neurol. 463:249-263.

Vigers AJ, Baquet ZC, Jones KR. 2000. Expression of neurotrophin-3 in the mouse forebrain: insights from a targeted LacZ reporter. J Comp Neurol 416:398-415.

Vogt BA. 1985. Cingulate cortex. In: Peters A, Jones EG, editors. Cerebral Cortex Vol. 4. Association and Auditory Cortices. New York: Plenum. p   89-149.

von Campenhausen H, Yoshihara Y, Mori K.   1997. OCAM   reveals   segregated mitral/tufted cell pathways in developing accessory olfactory bulb. Neuroreport. 8:2607-2612.

Walz A, Mombaerts P, Greer CA, Treloar HB. 2006. Disrupted compartmental organization of axons and dendrites within olfactory glomeruli of mice deficient in the olfactory cell adhesion molecule, OCAM. Mol Cell Neurosci. 32:1-14.

Wong RO, Ghosh A. 2002. Activity-dependent regulation of dendritic growth and patterning. Nat Rev Neurosci. 3:803-812.

Wyss JM, Van Groen T, Sripanidkulchai K. 1990. Dendritic bundling in layer I of granular retrosplenial cortex: intracellular labeling and selectivity of innervation. J Comp Neurol. 295:33-42.

Yamamoto T, Sakakibara S, Mikoshiba K, Terashima T. 2003. Ectopic corticospinal tract and corticothalamic tract neurons in the cerebral cortex of yotari and reeler mice. J Comp Neurol. 461:61-75.

Yoshihara Y, Kawasaki M, Tamada A, Fujita H, Hayashi H, Kagamiyama H, Mori K. 1997. OCAM: A new member of the neural cell adhesion molecule family related to zone-to-zone projection of olfactory and vomeronasal axons. J Neurosci. 17:5830-5842.